BIFURCATION ANALYSIS OF THE ECKHAUS INSTABILITY

Laurette S. TUCKERMAN
Department of Mathematics and Center for Nonlinear Dynamics, University of Texas, Austin, TX 78712, USA

and

Dwight BARKLEY
Program in Applied and Computational Mathematics, Princeton University, Princeton, NJ 08544, USA

The bifurcation diagram for the Eckhaus instability is presented, based on the Ginzburg–Landau equation in a finite domain with either free-slip or periodic boundary conditions. The conductive state is shown to undergo a sequence of destabilizing bifurcations giving rise to branches of pure-mode states; all branches but the first are necessarily unstable at onset. Each pure-mode branch undergoes a sequence of secondary restabilizing bifurcations, the last of which is shown to correspond to the Eckhaus instability. The restabilizing bifurcations arise from mode interactions between the pure-mode branches, and can be related directly to the destabilizing bifurcations of the conductive state. The downwards shift of the Eckhaus parabola calculated by Kramer and Zimmerman for the case of finite geometry is stressed. Through a center manifold reduction, it is proved that for the Ginzburg–Landau equation all restabilizing bifurcations of the pure-mode states are subcritical, and hence that the Eckhaus instability is itself subcritical.

1. Introduction

In many hydrodynamic systems, the first transition is from a uniform, featureless state to a long sequence of parallel rolls. If there is no variation along the roll axes, then by averaging or modeling over the roll depth, these flows can be described as one-dimensional and periodic. This is the simplest example of pattern formation, in which the "pattern" is specified merely by a wavelength.

In 1965, Eckhaus [1] proposed a general framework, using what is now called the Ginzburg–Landau equation, for studying such periodic states, in particular the dependence of their stability on wavelength. As a one-dimensional, analytically accessible phenomenon, the Eckhaus instability has since been instrumental in the derivation of model equations for hydrodynamics, from amplitude expansions to phase dynamics. In their classic articles, Newell and Whitehead [2] and Segel [3] derived amplitude equations for convection, which were later revised by Zippelius and Siggia [4] and further generalized by Cross and Newell [5]. Using an expansion in phase gradient rather than amplitude, Pomeau and Manneville [6] interpreted the Eckhaus instability as a change in sign of a longitudinal phase diffusion constant. Kramer and Zimmerman [7] performed a derivation of this kind starting from a general reaction-diffusion equation. Daniels [8], Cross et al. [9], and Zaleski et al. [10, 11] have considered boundary conditions appropriate for convection, and Riecke and Paap [12] numerically calculated the
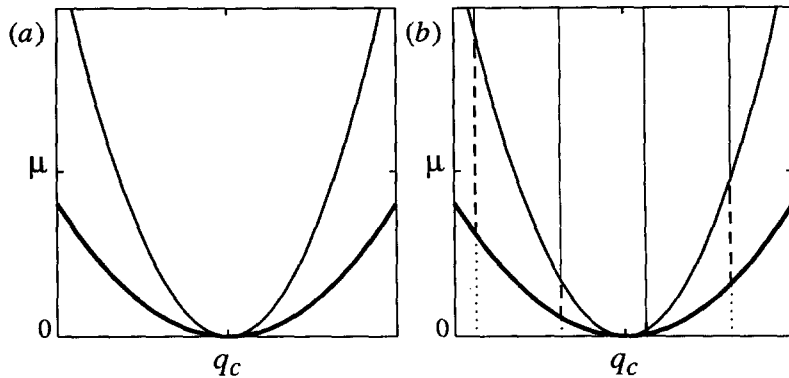
Fig. 1. The classic Eckhaus instability in an infinite domain. (a) The bold curve is the existence parabola $\mu = (q - q_c)^2$. Here q_c is the critical wavenumber at onset ($\mu = 0$) derived from linear stability analysis of the conductive state. Below the existence parabola, the conductive state is the only solution. Above this curve, the conductive state is unstable to perturbations of the form e^{iqx}, and solutions of this form exist. Above the existence parabola is the classic Eckhaus parabola $\mu = 3(q - q_c)^2$. According to the analysis of Eckhaus, solutions of the form e^{iqx} are unstable below this curve, and stable above it. Between the two curves are the Eckhaus bands, where solutions of the form e^{iqx} exist but are not stable. (b) Vertical lines have been added to indicate the quantization due to finite length. Only states along these lines have wavenumbers that are permitted by the boundary conditions. The dotted, dashed, and solid portions represent nonexistent, unstable, and stable solutions, respectively.

Eckhaus boundary far from transition. Coullet et al. [13] discuss the Eckhaus instability in the more general context of symmetry breaking. A more complete review of the considerable literature on the Eckhaus instability is beyond the scope of this article.

The behavior of the one-dimensional equation governing the Eckhaus instability in an infinite domain is illustrated in fig. 1a. For negative values of a control parameter μ, the only solution is the uniform or trivial state. At $\mu = 0$, the trivial solution loses stability to a periodic pattern of wavenumber q_c, i.e. of functional form $e^{iq_c x}$. At a slightly higher value of the control parameter, the trivial state is unstable to all periodic patterns e^{iqx} whose wavenumber q satisfies $(q - q_c)^2 \leq \mu$. However, these periodic solutions are themselves unstable, unless q falls in the smaller range $(q - q_c)^2 \leq \frac{1}{3}\mu$, a parabolic region in the (q, μ) plane bounded on both sides by the unstable regions called "Eckhaus bands".

The Eckhaus instability has been studied experimentally in Rayleigh–Bénard convection [14], Taylor–Couette flow [15], and in liquid crystals [16], by preparing a state with wavenumber $q \neq q_c$ at a control parameter μ at which it is stable, and lowering the value of μ until it falls into one of the Eckhaus bands. The rolls are then too narrow or too wide and the system abruptly gains or loses one or more rolls.

Although an infinite domain allows the calculation of closed-form solutions, it cannot be realized experimentally. One remedy is to pose the problem in a finite domain which is long compared to the "natural" wavelength $2\pi/q_c$ of the system. Either periodic or free-slip boundary conditions retain the analytic simplicity of the infinite domain. Although other boundary conditions are more convenient for experiments, such domains can in fact be realized: Croquette and Pocheau [14], for example, use a narrow annulus as a convection cell, satisfying periodic boundary conditions.

A finite domain is preferable for another reason as well: the spectra of linearized operators on finite domains are discrete (rather than continuous), permitting bifurcation-theoretic analysis. Bifurcation theory provides a comprehensive classification of the possible number and type of nonlinear solutions, based on the calculation of eigenvalues. It is a powerful and rigorous method of studying branching and stability, requiring little detailed knowledge of the equations and the functional form of the solutions.
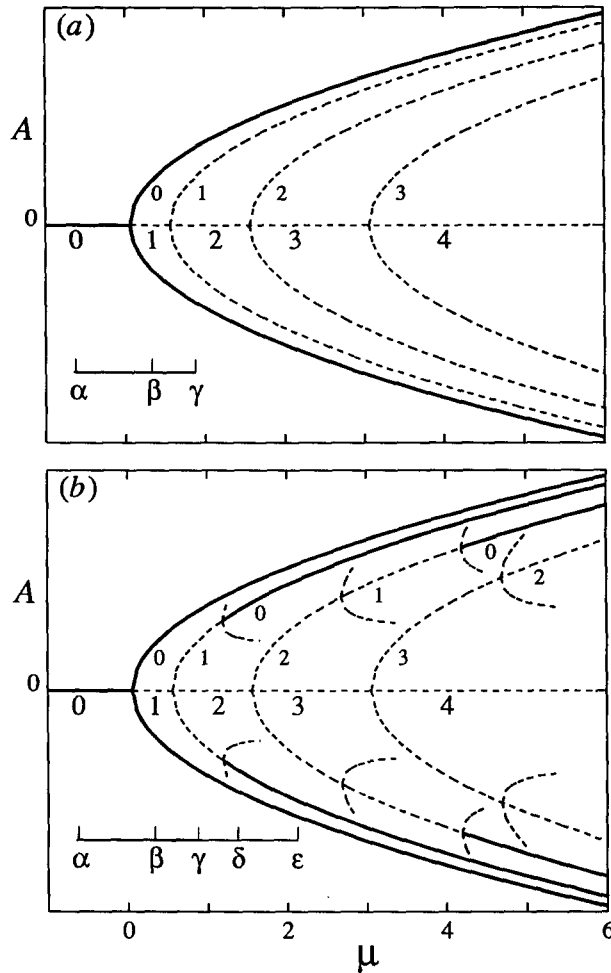
Fig. 2. Bifurcation diagrams. The horizontal axis is the control parameter μ; the vertical axis the amplitude $|A|$ of different states. Solid and dashed curves represent branches of stable and unstable steady states, respectively. Greek letters designate μ values for the phase portraits of fig. 3. Fig. 2a illustrates successive supercritical bifurcations creating branches of pure-mode states. Fig. 2b includes subcritical bifurcations to mixed-mode states which restabilize the pure-mode branches. Each of the trivial and pure-mode branches is labeled with its instability index. This index is defined in the text as the number of unstable directions, and changes with μ at each successive bifurcation. Note that the instability index of each branch A_n is equal to n when it first appears. The small extent in μ of the mixed-mode branches, as well as the omission of their indices, is for visual clarity.

Yet the Eckhaus instability has not been analyzed in bifurcation-theoretic terms. This analysis, which is the subject of the present paper, yields the following scenario.

In the finite periodic domain, the wavenumbers are restricted to the integer multiples of $2\pi/L$, as shown in fig. 1b. Solution branches A_n with different wavenumbers q_n are produced by supercritical pitchfork bifurcations, and appear successively as the control parameter μ is increased above zero. The bifurcation diagram, showing a quantity such as the amplitude modulus $|A|$ as a function of μ for the different branches is shown in fig. 2a.

The first bifurcation renders the trivial solution unstable, and all subsequent solutions bifurcating from the trivial solution are necessarily unstable. This had been conjectured by Segel [3] on the basis of
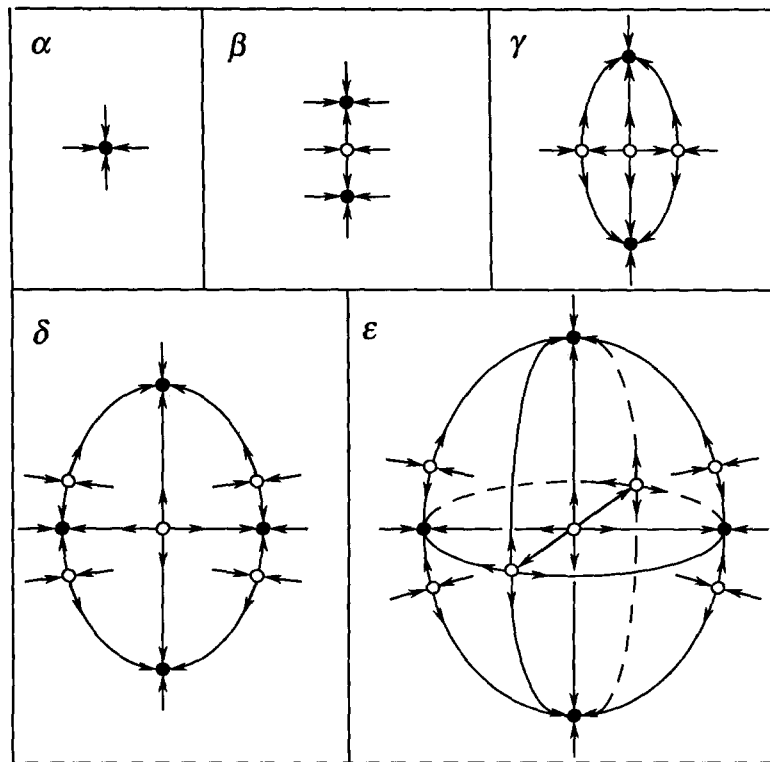
Fig. 3. Schematic phase portraits at various values of μ. The coordinates represent projections of the first two or three unstable directions of the conductive state C. Stable steady states are indicated by filled circles, unstable steady states by hollow circles. The values of μ are as indicted in fig. 2. (α) For $\mu < 0$, only the conductive state C exists. It is stable, as indicated by the solid circle and by the arrows pointing towards it. (β) After one supercritical bifurcation, C is unstable, and a pair of stable steady states A_0 (whose wavenumber is q_0, the allowed wavenumber closest to q_c) has been created. (γ) After a second supercritical bifurcation, C has two unstable directions. Another pair of steady states A_1, with allowed wavenumber q_1, now exists. These, however, are unstable (in one direction), as can be seen from the trajectories leading to the first pair of steady states A_0. These trajectories and unstable directions are inherited from C. (δ) States A_1 have been stabilized by undergoing a subcritical bifurcation. Each of the states A_1 emits a pair of unstable steady states, here located on the trajectories joining A_0 and A_1. (ε) C has undergone another supercritical bifurcation, acquiring a third unstable direction, and creating another pair of unstable steady states A_2. Each of these new states has two unstable directions, as can be seen from the trajectories joining A_2 to A_0 (toward the north and south poles) and to A_1 (left and right along the equator). States A_2 would require two subcritical bifurcations, one in each of the unstable directions, in order to become stable.

physical arguments. However, the bifurcation-theoretic reason for this instability is quite general: branches created by pitchfork bifurcation "inherit" the instabilities of their parent state (here the trivial state) at the moment of bifurcation. This is illustrated by the phase portraits of fig. 3 labeled α, β, and γ.

Thus successive pitchfork bifurcations cannot, by themselves, create multiple steady *stable* states. If the multiple states are to be observed, some process must intervene to render the branches stable. Such a process is shown in phase portrait δ of fig. 3. Here, the branches A_n have undergone further "secondary" pitchfork bifurcations. Each bifurcation stabilizes the branch A_n to one of its unstable directions, and is accompanied by the formation of additional unstable branches. Branch A_n, having n unstable directions at onset, must undergo n secondary bifurcations in order to become stable. The resulting bifurcation diagram is shown in fig. 2b, where each branch is labeled by the number of its

unstable directions. In this article, we will prove that this diagram is correct, and that the last of these bifurcations corresponds to the Eckhaus instability.

2. Derivation and scaling of the equations

We follow Newell and Whitehead [2], who derive a Ginzburg–Landau equation in the context of Rayleigh–Bénard convection. The Boussinesq equations govern the velocity w of a fluid subject to an externally imposed temperature gradient measured by the Rayleigh number Ra. The trivial solution $w = 0$ is called the conductive state and is linearly stable for Ra less than the critical Rayleigh number Ra_c, where it becomes unstable to a critical eigenfunction proportional to $e^{\pm iq_c x}$. Newell and Whitehead set:

$$Ra = Ra_c(1 + \epsilon^2 \mu).$$

The parameter ϵ is a measure of the order of magnitude of the deviation of Ra from criticality, so that μ is $\mathcal{O}(1)$. They then perform a multiple-scale analysis, valid near threshold ($\epsilon \ll 1$) and in a large container ($L \sim 1/\epsilon$), using the slowly varying variables

$$X = \epsilon x, \tag{2.1a}$$

$$T = \epsilon^2 t, \tag{2.1b}$$

the series expansion

$$w = \epsilon w_0 + \epsilon^2 w_1 + \epsilon^3 w_2 + \dots,$$

and a complex amplitude function $A(X, T)$ such that

$$w_0(x, t) = A(X, T) e^{iq_c x} + A^*(X, T) e^{-iq_c x} = 2 \operatorname{Re}\left[A(X, T) e^{iq_c x} \right]. \tag{2.2}$$

At order ϵ^3, the following solvability condition is derived:

$$\tau_0 \frac{\partial A}{\partial T} = \mu A + \xi_0^2 \frac{\partial^2 A}{\partial X^2} - |A|^2 A, \tag{2.3}$$

where τ_0 and ξ_0^2 are physical temporal and spatial scales.

At this point, A, T, and X are often rescaled to make all the coefficients in (2.3) unity (e.g. refs. [2, 7, 9]). However, our treatment will now begin to differ from the classic one. We wish to investigate the effects of a finite geometry, and also to vary μ. We will impose Neumann boundary conditions – "free-slip" in the language of convection – on the original velocity w, in a domain of length $L/2$:

$$\frac{\partial w_0}{\partial x} = 0 \quad \text{at } x = 0, L/2.$$

Referring to (2.1a) and (2.2), this implies the following boundary conditions for A:

$$\frac{\partial}{\partial x}\text{Re}\left[A(\epsilon x)\,e^{iq_c x}\right] = 0 \quad \text{at } x = 0, L/2.$$

We will also consider periodic boundary conditions on w over a domain of length L:

$$w_0(x+L) = w_0(x).$$

Referring to (2.1a) and (2.2), this implies the following boundary conditions for A:

$$A(\epsilon(x+L))\,e^{iq_c L} = A(\epsilon x).$$

The boundary conditions can be put in a more convenient form if we introduce rescaled variables as follows:

$$\tilde{x} \equiv \frac{2\pi}{L}x = \frac{2\pi}{\epsilon L}X, \tag{2.4}$$

$$\tilde{A}(\tilde{x}) \equiv \frac{\epsilon L}{2\pi\xi_0}A\left(\frac{\epsilon L}{2\pi}\tilde{x}\right) = \frac{\epsilon L}{2\pi\xi_0}A(X), \tag{2.5}$$

$$Q_c \equiv \frac{q_c L}{2\pi}, \tag{2.6}$$

leading to the desired form for the free-slip boundary conditions:

$$\frac{\partial}{\partial \tilde{x}}\text{Re}\left[A(\tilde{x})\,e^{iQ_c\tilde{x}}\right] = 0 \quad \text{at } \tilde{x} = 0, \pi, \tag{2.7}$$

as well as for the periodic boundary conditions:

$$\tilde{A}(\tilde{x}+2\pi)\,e^{i2\pi Q_c} = \tilde{A}(\tilde{x}). \tag{2.8}$$

We substitute (2.4) and (2.5) into (2.3), obtaining the equation

$$\tau_0\left(\frac{\epsilon L}{2\pi\xi_0}\right)^2\frac{\partial \tilde{A}}{\partial T} = \mu\left(\frac{\epsilon L}{2\pi\xi_0}\right)^2\tilde{A} + \frac{\partial^2\tilde{A}}{\partial \tilde{x}^2} - |\tilde{A}|^2\tilde{A}.$$

Finally, introducing

$$\tilde{t} \equiv \frac{1}{\tau_0}\left(\frac{2\pi\xi_0}{\epsilon L}\right)^2 T, \tag{2.9}$$

$$\tilde{\mu} \equiv \mu\left(\frac{\epsilon L}{2\pi\xi_0}\right)^2, \tag{2.10}$$

we arrive at

$$\frac{\partial \tilde{A}}{\partial \tilde{t}} = \tilde{\mu}\tilde{A} + \frac{\partial^2\tilde{A}}{\partial \tilde{x}^2} - |\tilde{A}|^2\tilde{A}. \tag{2.11}$$

The scaled velocity $\tilde{w}$ corresponding to $\tilde{A}$ is

$$\tilde{w}(\tilde{x},\tilde{t}) = 2\,\mathrm{Re}\big[\tilde{A}(\tilde{x},\tilde{t})\,e^{iQ_c\tilde{x}}\big].$$

Since the remainder of the paper will discuss the dependence of the solutions on Q_c and $\tilde{\mu}$, it is appropriate to emphasize what these parameters signify in terms of the original variables of the system. Since $2\pi/q_c$ is the critical wavelength, i.e. the wavelength preferred by the system at $\mu = 0$, we see from (2.6) that Q_c measures the number – usually non-integer – of such waves that would fit in a container of size L. For example, in convection with free-slip boundaries, $q_c = \pi/\sqrt{2}$, so that $Q_c = L/2\sqrt{2}$. We assume a long container, so that $Q_c \gg 1$.

It is worth noting that μ appears only in the definition (2.10) of $\tilde{\mu}$. The usual scalings

$$\tilde{X} \equiv \frac{\sqrt{\mu}}{\xi_0} X, \qquad \tilde{A} \equiv \frac{1}{\sqrt{\mu}} A, \qquad \tilde{T} \equiv \frac{\mu}{\tau_0} T$$

used to set all coefficients of (2.3) to unity become singular when μ is zero or negative, whereas definitions (2.4), (2.5), (2.9) for $\tilde{x}$, $\tilde{A}$, and $\tilde{t}$ allow us to consider $\mu \leq 0$.

The procedure employed in the preceding derivation is to derive the partial differential equation valid near threshold in an infinite domain, and then to impose boundary conditions. As pointed out by Matkowsky [16], a more rigorous treatment of the Eckhaus instability in realistic fluid-dynamical systems would reverse this order, considering the Boussinesq equations themselves in a finite domain, thus discretizing the number of modes, and then deriving a set of coupled ordinary differential equations (rather than a partial differential equation) for the amplitudes of these modes, valid near threshold. The scaling (2.4), (2.5), (2.9) has also been used by Daniels [8]; he and other authors [3, 9–11] have studied convection in domains with rigid or imperfectly insulating boundaries, using the techniques of boundary layers and matched asymptotics. Eq. (2.7) has also been generalized to include three-dimensional effects [2, 4–6]. We will not consider any of these physically realistic but complicating factors here, choosing instead to take equations (2.10) and either (2.7) or (2.8) as given.

Henceforth, we drop the tildes and revert to using the notation A, x, t, w and μ.

3. Quantization and branching of the pure-mode states

We have now set up our problem and equations:

$$\frac{\partial A}{\partial t} = \mu A + \frac{\partial^2 A}{\partial x^2} - |A|^2 A. \tag{3.1}$$

For simplicity, we will consider primarily the free-slip boundary conditions:

$$\frac{\partial}{\partial x}\mathrm{Re}\big[A(x,t)\,e^{iQ_c x}\big] = 0 \quad \text{at } x = 0, \pi \tag{3.2}$$

and will postpone extensions to the case of periodic boundary conditions:

$$A(x + 2\pi, t)\,e^{iQ_c 2\pi} = A(x,t) \tag{3.3}$$

Table 1
Summary of notation

	Conductive	Pure mode	Mixed
branches	$C = 0$	$A_n = \sqrt{\mu - Q_n^2}\, e^{iQ_n x}$	S_{nk}
eigenvectors	$c_n = e^{iQ_n x}$	$a_{n0} = e^{iQ_n x}$ $a_{nk+} = e^{iQ_n x}\left(\alpha_{nk} e^{ikx} + \beta_{nk} e^{-ikx}\right)$ $a_{nk-} = e^{iQ_n x}(\beta_{nk} e^{ikx} - \alpha_{nk} e^{-ikx})$	
eigenvalues	$\lambda_n = \mu - Q_n^2$	$\sigma_{n0} = \sigma_0(Q_n, \mu) = -2(\mu - Q_n^2)$ $\sigma_{nk+} = \sigma_+(Q_n, k, \mu) = -\left(\mu - Q_n^2 - k^2\right) + \sqrt{\left(\mu - Q_n^2\right)^2 + (2kQ_n)^2}$ $\sigma_{nk-} = \sigma_-(Q_n, k, \mu) = -(\mu - Q_n^2 - k^2) - \sqrt{\left(\mu - Q_n^2\right)^2 + (2kQ_n)^2}$	
critical points	$\mu_n = Q_n^2$	$\mu_{n0} = Q_n^2$ $\mu_{nk} = \mu^E(Q_n, k) = 3Q_n^2 - \tfrac{1}{2}k^2$	

to a later section. We also recall the definition:

$$w(x,t) = 2\,\mathrm{Re}\left[A(x,t)\, e^{iQ_c x}\right]. \tag{3.4}$$

It is easily verified that one solution to (3.1)–(3.2) is $A = 0$, which we shall call C, or the "conductive branch", borrowed from the Rayleigh–Bénard context. Table 1 lists all of the notation which we shall introduce. At $\mu = Q^2$, C becomes unstable to an eigenvector of the form e^{iQx}, as can be seen by substituting $e^{iQx} e^{\lambda t}$ into the linearization of (3.1) about C to obtain

$$\lambda = \mu - Q^2.$$

For $\mu \geq Q^2$, there exist steady solutions, sometimes called "pure modes":

$$A = \sqrt{\mu - Q^2}\, e^{i\phi} e^{iQx}. \tag{3.5}$$

Referring to eq. (3.4), we see that the fluid velocity w has total wavenumber $q = Q + Q_c$. This explains the lack of equivalence between Q and $-Q$, which describe wavenumbers larger, or smaller, than Q_c, respectively. Note that by eq. (3.4) it is possible for one state w to be represented by two different values Q, Q' if

$$Q + Q_c = -(Q' + Q_c).$$

We prevent this by requiring q to be positive, restricting the size of the wavenumbers Q:

$$|Q| < Q_c,$$

where we recall that the Q_c defined in (2.6) is assumed to be very large.

We now focus on the effect of the boundary conditions. Either of the boundary conditions (3.2) or (3.3) imply the quantization

$$Q + Q_c = \text{integer} \tag{3.6}$$

Table 2

Allowed wavenumbers for the case $Q_c = N - \frac{1}{4}$. The set of allowed wavenumbers depends on the rescaled Q_c defined in (2.6), i.e. the number of preferred wavelengths that would fit in a container of length L. The boundary conditions (3.2) or (3.3) allow only solutions A_n whose wavenumbers Q_n differ from Q_c by an integer. The allowed wavenumbers are shown in the order of their bifurcation from C, i.e. in order of increasing critical value μ_n. Branch A_n has n unstable directions at onset, inherited from C. Also shown are the values of integers k which index the restabilizing bifurcations and the critical values μ_{nk} at which these take place. The final ($k = 1$) restabilizing bifurcation is the Eckhaus instability which separates the unstable and stable portions of branch A_n. Each restabilizing bifurcation of A_n can be shown to correspond to a destabilizing bifurcation of C with wavenumber Q_m (see (5.2); this m is indicated in the last column. The typical example $Q_c = N - \frac{1}{4}$ was used in formulating the figures.

n	Q_n	$\mu_n = Q_n^2$	$k \le 2\lvert Q_n \rvert$	μ_{nk}	Restabilized m
0	1/4	1/16	none		
1	−3/4	9/16	1	19/16	0
2	5/4	25/16	2	43/16	1
			1	67/16	0
3	−7/4	49/16	3	75/16	2
			2	115/16	0
			1	139/16	1
4	9/4	81/16	4	115/16	3
			3	171/16	1
			2	211/16	0
			1	235/16	2

for both the eigenvector and the pure-mode solution. Free-slip boundary conditions (3.2) lead to the additional requirement that ϕ in (3.5) equal 0 or π. Thus for every allowed wavenumber Q, there exists a pair of solutions. The multiplicity of solutions is due to the reflection symmetry of the domain, and implies that the bifurcations producing states A are of pitchfork type. In the analysis of the text, we generally fix $\phi = 0$, which will not affect the results.

We see from (3.6) that the allowed values of Q (see tables 2–5) are not integers (except in the unusual case that Q_c is itself an integer, meaning that the favored wavelength fits exactly into the container), but numbers which differ from $-Q_c$ by an integer. The allowed values of Q may be listed in increasing order of appearance, i.e. in increasing order of Q^2, beginning with Q_0. Both of the values $\pm Q$ are permitted only if Q_c is an integer or a half-integer: then, we adopt the convention that the positive value of Q is listed first.

Table 2 lists the allowed values of Q_n for the case $Q_c = N - \frac{1}{4}$ (N integer), to serve as an example. This is the set of allowed wavenumbers used to generate figs. 1b, 2, 4, and 7. In the general case shown in table 3, Q_c is neither integer nor half-integer, and we can write

$$Q_c = N + l, \quad \text{with } N \text{ integer and } 0 < \lvert l \rvert < \tfrac{1}{2}, \tag{3.7a}$$

where

$$l \equiv \left[\left(Q_c + \tfrac{1}{2} \right) \bmod 1 \right] - \tfrac{1}{2}. \tag{3.7b}$$

We see that $\lvert Q_{2n} \rvert = n + \lvert l \rvert$ while $\lvert Q_{2n+1} \rvert = n + 1 - \lvert l \rvert$. Hence $2\lvert Q_{2n} \rvert = 2n + 2\lvert l \rvert$ and $2\lvert Q_{2n+1} \rvert = 2n + 2 - 2\lvert l \rvert$. The inequality $0 < 2\lvert l \rvert < 1$ then implies that

$$2n < 2\lvert Q_{2n} \rvert < 2n + 1 < 2\lvert Q_{2n+1} \rvert < 2n + 2$$

Table 3
Allowed wavenumbers for the general case $Q_c = N + l$ with $0 < |l| < \frac{1}{2}$. See table 2 for caption, and eq. (3.7) for definition of l. Upper and lower signs refer to positive and negative values of l, respectively.

n	Q_n	$\mu_n = Q_n^2$	$k \leq 2|Q_n|$	μ_{nk}	Restabilized m
0	l	l^2	none		
1	$l \mp 1$	$(l \mp 1)^2$	1	$3(l \mp 1)^2 - \frac{1}{2}$	0
2	$l \pm 1$	$(l \pm 1)^2$	2	$3(l \pm 1)^2 - 2$	1
			1	$3(l \pm 1)^2 - \frac{1}{2}$	0
3	$l \mp 2$	$(l \mp 2)^2$	3	$3(l \mp 2)^2 - \frac{9}{2}$	2
			2	$3(l \mp 2)^2 - 2$	0
			1	$3(l \mp 2)^2 - \frac{1}{2}$	1
4	$l \pm 2$	$(l \pm 2)^2$	4	$3(l \pm 2)^2 - 8$	3
			3	$3(l \pm 2)^2 - \frac{9}{2}$	1
			2	$3(l \pm 2)^2 - 2$	0
			1	$3(l \pm 2)^2 - \frac{1}{2}$	2

and more generally, for every n, that

$$n < 2|Q_n| < n + 1. \tag{3.8}$$

Finally, the allowed values of Q_n for Q_c integer and half-integer are shown in tables 4 and 5, respectively.

We now introduce some notation based on the ordered wavenumbers Q_n. The eigenvalue that becomes positive at $\mu = Q_n^2$ is denoted

$$\lambda_n(\mu) \equiv \mu - Q_n^2. \tag{3.9}$$

The critical value of μ at which $\lambda_n(\mu)$ becomes positive is denoted

$$\mu_n \equiv Q_n^2 \tag{3.10}$$

Table 4
Allowed wavenumbers for Q_c integer. See table 2 for caption. Wavenumbers $\pm Q_n$ with the same absolute value are described on one line.

n	Q_n	$\mu_n = Q_n^2$	$k \leq 2|Q_n|$	μ_{nk}	Restabilized m
0	0	0	none		
1, 2	± 1	1	2	1	1, 2
			1	2.5	0, 0
3, 4	± 2	4	4	4	4, 3
			3	7.5	2, 1
			2	10	0, 0
			1	11.5	1, 2
5, 6	± 3	9	6	9	6, 5
			5	14.5	4, 3
			4	19	2, 1
			3	22.5	0, 0
			2	25	1, 2
			1	26.5	3, 4

Table 5

Allowed wavenumbers for Q_c half-integer. See table 2 for caption. Wavenumbers $\pm Q_n$ with the same absolute value are described on one line.

n	Q_n	$\mu_n = Q_n^2$	$k \leq 2|Q_n|$	μ_{nk}	Restabilized m
0, 1	± 0.5	0.25	1	0.25	1, 0
2, 3	± 1.5	2.25	3	2.25	3, 2
			2	4.75	1, 0
			1	6.25	0, 1
4, 5	± 2.5	6.25	5	6.25	5, 4
			4	10.75	3, 2
			3	14.25	1, 0
			2	16.75	0, 1
			1	18.25	2, 3

with corresponding eigenvector

$$c_n \equiv e^{iQ_n x}. \tag{3.11}$$

The branch with wavevector Q_n which exists for $\lambda_n \geq 0$, i.e. for $\mu \geq \mu_n = Q_n^2$, is denoted by

$$A_n(\mu) \equiv \sqrt{\mu - Q_n^2} \, e^{iQ_n x}. \tag{3.12}$$

(All the notation is summarized in table 1.) For simplicity, we will generally omit the argument μ when it is clear from the context.

For Q_c neither integer nor half-integer, as μ is increased, one eigenvalue λ_n crosses zero at each bifurcation point μ_n. Similarly, the solution branches A_n appear one at a time. This sequence of events is summarized by the bifurcation diagram in fig. 2a.

For $\mu > \mu_{n-1}$, we have $\lambda_{n-1} > 0$. Since $\lambda_0 \geq \lambda_1 \geq \ldots \geq \lambda_{n-1}$, it follows that C has n positive eigenvalues, with n corresponding unstable directions. For example, in fig. 3γ, C has zero unstable directions in phase portrait 3α, one in phase portrait 3β, two in 3γ and 3δ, and three unstable directions, in 3ε. Surprisingly, there seems to be no simple word in common usage for this number, despite the widespread applicability of the concept. The well-known Leray–Schauder index [18] is defined to be $(-1)^n$ in this case, and therefore conveys only the parity of n. One can say that the unstable manifold of C is n-dimensional (e.g. refs. [19, 20]). Palis and de Melo [21] define an index which is the number of *negative* eigenvalues; we shall use the term "instability index" to denote the number of *positive* eigenvalues. In the absence of pathology, a bifurcating branch will inherit the unstable directions of its parent state C at the moment of bifurcation (more specifically, it will have the instability index of the portion of the parent state for μ values where the bifurcating branch does not yet exist). Thus A_n, with critical value $\mu = \mu_n > \mu_{n-1}$, will have an instability index of n when it first appears. In the next section, we shall demonstrate this explicitly, and we shall also follow the subsequent evolution of the instability index of A_n as μ is increased.

4. The Eckhaus instability

We now seek to calculate the stability of the solutions A_n defined by (3.12). We will find it convenient first to derive the results for a state $A = \sqrt{\mu - Q^2}\, e^{iQx}$ with arbitrary wavenumber Q; we shall re-introduce the discrete wavenumbers Q_n shortly. Perturbing about this steady state, we substitute $A + a$ into eq. (3.1), to derive the following equation for a:

$$\frac{\partial a}{\partial t} = \mu a + \frac{\partial^2 a}{\partial x^2} - 2|A|^2 a - A^2 a^* - \left(2A|a|^2 + A^* a^2 + |a|^2 a\right). \tag{4.1}$$

Setting $a = a(x)e^{\sigma t}$ and neglecting the nonlinear terms in parentheses, we get

$$\sigma a = \mu a + \frac{\partial^2 a}{\partial x^2} - 2|A|^2 a - A^2 a^*. \tag{4.2}$$

Nontrivial solutions to (4.2) are of the form

$$a(x) = e^{iQx}\left(\alpha\, e^{ikx} + \beta\, e^{-ikx}\right) \tag{4.3}$$

with α and β real, and $k \neq 0$. (We shall treat the case $k = 0$ below.) The requirement that α and β be real is derived from (3.2) and will be discussed in section 7. Since k and $-k$ appear symmetrically in (4.3), we take $k > 0$ without loss of generality.

Substituting (4.3) into (4.2), we obtain

$$\sigma\left(\alpha\, e^{ikx} + \beta\, e^{-ikx}\right)e^{iQx}e^{\sigma t}$$

$$= \left\{\mu(\alpha\, e^{ikx} + \beta\, e^{-ikx}) - \left[\alpha(Q+k)^2 e^{ikx} + \beta(Q-k)^2 e^{-ikx}\right]\right.$$

$$\left. -2(\mu - Q^2)(\alpha\, e^{ikx} + \beta\, e^{-ikx}) - (\mu - Q^2)(\alpha\, e^{-ikx} + \beta\, e^{ikx})\right\}e^{iQx}e^{\sigma t}.$$

We separate the two functional forms $e^{i(Q+k)x}$ and $e^{i(Q-k)x}$:

$$\begin{pmatrix} \sigma & 0 \\ 0 & \sigma \end{pmatrix}\begin{pmatrix} \alpha \\ \beta \end{pmatrix} = -\begin{pmatrix} \mu - Q^2 + k^2 + 2kQ & \mu - Q^2 \\ \mu - Q^2 & \mu - Q^2 + k^2 - 2kQ \end{pmatrix}\begin{pmatrix} \alpha \\ \beta \end{pmatrix} \tag{4.4}$$

and solve for the eigenvalues,

$$\sigma_\pm(Q, k, \mu) = -\left(\mu - Q^2 + k^2\right) \pm \sqrt{\left(\mu - Q^2\right)^2 + (2kQ)^2}. \tag{4.5}$$

There is an additional eigenvalue and eigenvector, corresponding to $k = 0$. Substituting $a = e^{iQx}$ into (4.2), we obtain the single eigenvalue

$$\sigma_0(Q, \mu) = -2(\mu - Q^2). \tag{4.6}$$

Let us now discuss the significance of these eigenvalues. We see that neither σ_- nor σ_0 can ever be positive (for $\mu > Q^2$), so that only σ_+ has the potential for causing instability. The values of μ at which

$\sigma_+ = 0$ are points of bifurcation and are readily calculated by solving

$$0 = -\left(\mu - Q^2 + k^2\right) + \sqrt{\left(\mu - Q^2\right)^2 + (2kQ)^2}. \tag{4.7}$$

We define the k-parabolas $\mu^E(Q, k)$ as the solutions to (4.7):

$$\mu^E(Q, k) \equiv 3Q^2 - \tfrac{1}{2}k^2. \tag{4.8}$$

Since $\sigma_+(Q, k, \mu) \leq 0$ if and only if $\mu \geq \mu^E(Q, k)$, the state with wavenumber Q is stable if and only if $\sigma_+(Q, k, \mu) \leq 0$ for all possible k, i.e. if and only if

$$\mu \geq \sup_{k>0} \mu^E(Q, k) = \sup_{k>0}\left(3Q^2 - \tfrac{1}{2}k^2\right). \tag{4.9}$$

By allowing k to tend to zero, one obtains $\mu \geq 3Q^2$. This is the well-known Eckhaus parabola

$$\mu = \mu^E(Q, 0) = 3Q^2 \tag{4.10}$$

located inside (above) the parabola $\mu = Q^2$ delimiting the instability of the conductive state C; both of these curves are shown in fig. 1a.

It is important to emphasize that the classic instability limit (4.10) is derived from the eigenvalue σ_+ by taking the limit $k \to 0^+$ implied by (4.9):

$$\sigma_+\left(Q, k, \mu = 3Q^2\right) = 2Q^2\left(-1 - k^2/2Q^2 + \sqrt{1 + k^2/Q^2}\right) \to 0 \quad \text{as } k \to 0^+$$

and not from the eigenvalue (4.6) corresponding to setting $k = 0$:

$$\sigma_0\left(Q, \mu = 3Q^2\right) = -4Q^2 < 0.$$

(The eigenvalue σ_- coalesces with σ_0 as $k \to 0^+$.) We also stress that the eigenvector (4.3) associated with the Eckhaus instability is a linear combination of states with wavenumber $Q \pm k$; small k values thus correspond to a linear combination of wavenumbers close to Q.

The analysis up until this point can be found in various forms in refs. [1, 2], and many subsequent sources (e.g. ref. [13]). However, we now return to our investigation of the effects of finite, albeit large, geometry. To begin with, either of the boundary condition (3.2) or (3.3) lead to quantization of k. Since both $Q_c + Q + k$ and $Q_c + Q$ must be integers, k must be an integer. We define

$$\mu_{nk} \equiv \mu^E(Q_n, k) = 3Q_n^2 - \tfrac{1}{2}k^2, \tag{4.11}$$

$$\sigma_{n0}(\mu) \equiv \sigma_0(Q_n, \mu) = -2\left(\mu - Q_n^2\right), \tag{4.12}$$

$$\sigma_{nk\pm}(\mu) \equiv \sigma_\pm(Q_n, k, \mu) = -\left(\mu - Q_n^2 + k^2\right) \pm \sqrt{\left(\mu - Q_n^2\right)^2 + (2kQ_n)^2}. \tag{4.13}$$

The corresponding normalized eigenvectors are

$$a_{n0}(\mu) = e^{iQ_n x}, \tag{4.14}$$

$$a_{nk+}(\mu) \equiv e^{iQ_n x}\left[\alpha_{nk}(\mu)\, e^{ikx} + \beta_{nk}(\mu)\, e^{-ikx}\right], \tag{4.15a}$$

$$a_{nk-}(\mu) \equiv e^{iQ_n x}\left[\beta_{nk}(\mu)\, e^{ikx} - \alpha_{nk}(\mu)\, e^{-ikx}\right], \tag{4.15b}$$

where the coefficients α_{nk} and β_{nk} satisfy an equation derived from (4.4) and (4.13):

$$\begin{pmatrix} \sqrt{(\mu - Q_n^2)^2 + (2kQ_n)^2} + 2kQ_n & \mu - Q_n^2 \\ \mu - Q_n^2 & \sqrt{(\mu - Q_n^2)^2 + (2kQ)^2} - 2kQ_n \end{pmatrix} \begin{pmatrix} \alpha_{nk}(\mu) \\ \beta_{nk}(\mu) \end{pmatrix} = \begin{pmatrix} 0 \\ 0 \end{pmatrix}. \qquad (4.16)$$

Now k cannot become arbitrarily small; the smallest value that k can take is 1. Thus we see from (4.9) that the state of wavenumber Q is stable for $\mu > 3Q^2 - \frac{1}{2}$, and the location of the Eckhaus parabola is shifted downwards to

$$\mu = \mu^E(Q, 1) = 3Q^2 - \frac{1}{2}. \qquad (4.17)$$

It is important to note that this deviation of $\frac{1}{2}$ from the classic result (4.10) *is constant: it does not disappear asymptotically as the size L of the container becomes large.* This stabilizing effect of finite geometry was also calculated by Kramer and Zimmerman [7]. Their assumption that only k, and not Q, was quantized, led them to conclude that "the system becomes Eckhaus stable in the full band of existence" $Q^2 < \mu$ for L sufficiently small. However, Ahlers et al. [15] noticed that the finite length in fact created a "gap" in Q in which the Eckhaus instability becomes irrelevant, and whose width was such as to include exactly one allowed wavenumber. This allowed wavenumber is that closest to Q_c, which we have called Q_0.

We can generalize this claim as follows. The bifurcations at μ_{nk} can occur only if the state with wavenumber Q_n exists at this value of μ. That is, we require

$$\mu_n \le \mu_{nk}.$$

Using definitions (3.10) and (4.11), this becomes

$$Q_n^2 \le 3Q_n^2 - \frac{1}{2}k^2,$$

implying

$$k \le 2|Q_n|, \qquad (4.18)$$

where we have used the fact that $k > 0$.

For Q_c neither integer nor half-integer, inequality (3.8) locates $2|Q_n|$ between n and $n + 1$. Hence the inequality $k \le 2|Q_n|$ becomes simply $k \le n$ (see tables 2 and 3). Thus, the branch A_n undergoes exactly n "restabilizing bifurcations", at the μ values $\mu = \mu_{nk}$. The branch A_0 undergoes no restabilizing bifurcation, since no positive integer k satisfies $k \le 2|Q_0| < 1$: it is already stable. Note that the number of restabilizing bifurcations for each of the branches is precisely that required for the scenario described in section 1.

It is convenient to illustrate these results by graphing the k-parabolas $\mu = \mu^E(Q, k)$ defined in (4.6) in the (Q, μ) plane, as in fig. 4. The intersections of these parabolas with the vertical lines $Q = Q_n$ are the bifurcation points (Q_n, μ_{nk}). The k-parabola is irrelevant wherever it is below the existence parabola $\mu = Q^2$, i.e. wherever $k > 2|Q|$, or $k > 2|Q_n| \ge n$: this is its "gap". The gap of the $(k + 1)$-parabola accommodates exactly one more allowed wavenumber (Q_k) than does its predecessor, the k-parabola. Conversely, each successive wavenumber Q_{n+1} undergoes one more restabilizing bifurcation (with $k = n + 1$) than the wavenumber Q_n which precedes it.

For Q_c integer or half-integer, (4.18) still holds, although (3.8) does not. Instead (except for the case $Q_n = 0$), the allowed wavenumbers occur in pairs $\pm |Q|$, whose simultaneous bifurcation from C constitute multiple bifurcation points. Each member of the pair undergoes the same number of restabilizing bifurcations, and the number of restabilizing bifurcations increases by two for each successive pair. For these exceptional cases, it can be seen from tables 4 and 5 that for each n, there exists a k (either $k = n$ or $k = n + 1$, depending on the parity of n) for which $\mu_n = \mu_{nk}$. That is, one of the restabilizing bifurcations occurs simultaneously with the primary bifurcation creating A_n. These features are also illustrated in fig. 5, which displays all critical values μ_n and μ_{nk} as functions of l, defined in (3.7).

The mathematical necessity for the existence of the secondary restabilizing bifurcations, can, surprisingly, be understood from these exceptional cases of Q_c integer or half-integer. As was first suggested by Bauer, Keller, and Reiss [22] and studied in more detail by other authors [19, 23], multiple bifurcation points give rise to a combination of several simple primary and secondary bifurcation points as a
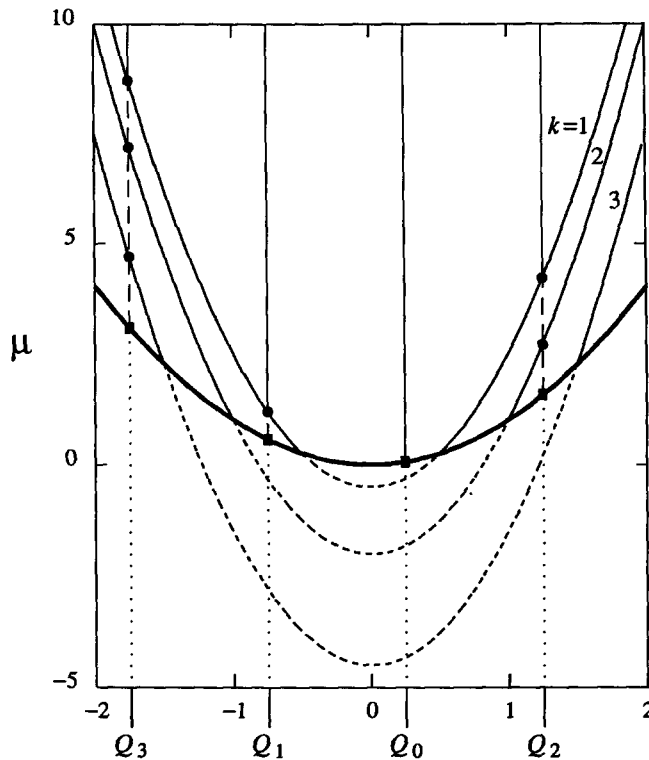

Fig. 4. The Eckhaus k-parabolas. As in fig. 1, the bold curve is the existence parabola $\mu = Q^2$. The first three Eckhaus parabolas $\mu^E(Q, k) = 3Q^2 - \frac{1}{2}k^2$, for $k = 1, 2$, and 3 are represented as solid curves. The bifurcations at μ_n (μ_{nk}) are represented by squares (circles) at the intersections of the existence parabola (Eckhaus parabolas) with the vertical lines $Q = Q_n$. The dotted, dashed, and solid portions of the vertical lines represent nonexistent, unstable, and stable solutions, respectively. The highest ($k = 1$) parabola separates the stable and unstable regimes (except for branch A_0); note the downwards shift from fig. 1b. The dashed portion of each Eckhaus parabola is "irrelevant", i.e. falls below the existence parabola $\mu = Q^2$. Note that each k-parabola is relevant only to wavenumbers Q_n satisfying $k \le n$; conversely wavenumber Q_n undergoes n restabilizing bifurcations.
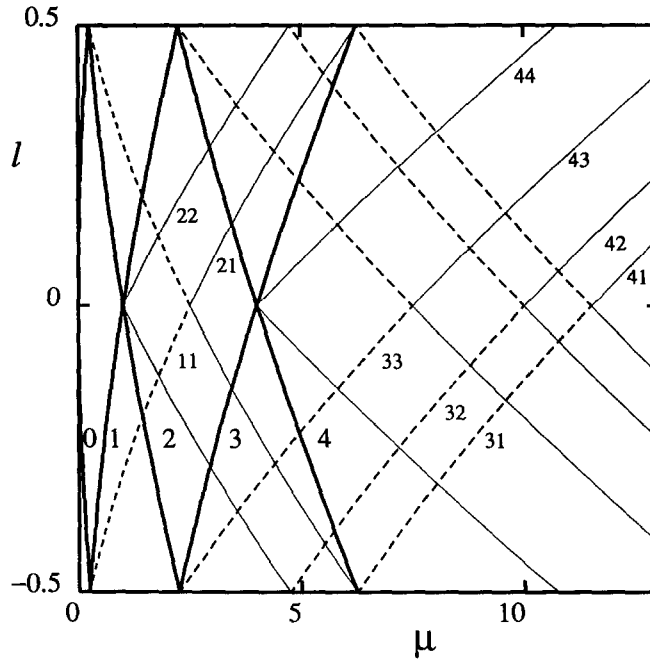
Fig. 5. Critical μ values as a function of l. Each bold curve shows the variation with l of μ_n, the critical value for the primary bifurcation to a pure-mode state of wavenumber Q_n; its label n is to the right of the corresponding curve. The thin curves show μ_{nk}, the locus of the kth secondary restabilizing bifurcation of the nth primary branch, and are labeled by the two integers n, k, again to the right of the curves. For clarity, solid thin curves correspond to even n, dashed curves to odd n. The symmetry of the graph, and the angles formed by the curves, are due to the fact that all the critical values depend only on $|l|$, as can be seen from the formulas in table 3. Multiple bifurcation points occur for $l = 0$ and $l = \pm\frac{1}{2}$, when μ_n intersects μ_{n+1}. Each multiple bifurcation is accompanied by the collision of the secondary bifurcations at μ_{nk} with those at $\mu_{n+1,k}$ and by the creation of new secondary bifurcations.

"splitting parameter" – here, Q_c or l – is varied. These secondary points move along one or more of the primary branches as Q_c varies. Thus the secondary restabilizing bifurcations, including the final Eckhaus bifurcation, arise as a necessary consequence of the simple fact that, for some particular geometries, two pure-mode branches can appear simultaneously at the same value of μ. The motion of the secondary bifurcations and their generation by the intersection of two primary branches can easily be traced in fig. 5.

Each secondary restabilizing bifurcation creates new steady states S_{nk}, sometimes called mixed-mode, or saddle-point solutions. These states have been studied, via a fruitful analogy to a particle in a central potential, by Newell and Whitehead [2], and by later authors (e.g. refs. [7, 9, 10, 11, 24]), and shown to be elliptic functions. In fig. 2b, we have represented all of the S_{nk} states as unstable, and as branching to the right of the bifurcation point. These two properties are related by the inheritance of instability indices: if the S_{nk} states branch to the right of μ_{nk}, then they inherit the instability indices (all positive) of the pure-mode states to the left of μ_{nk}. However, from the linear analysis carried out in this section, it is not possible to determine the direction of branching of the mixed-mode states. In the next section, we will show, by a higher-order calculation, that the branching direction is indeed as shown in fig. 2b.
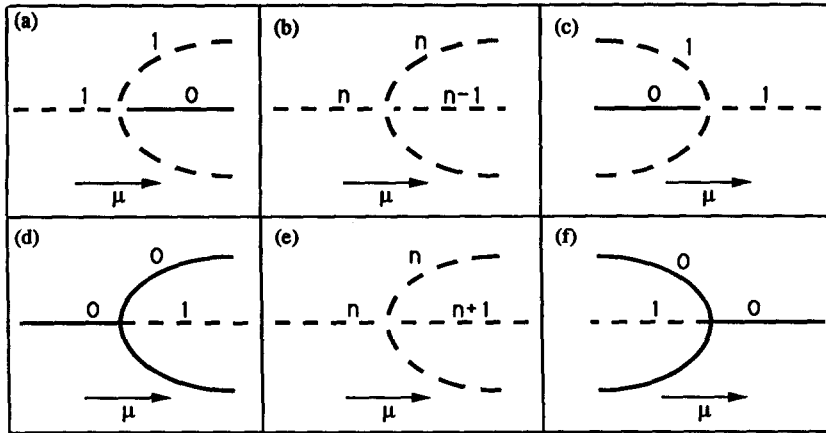
Fig. 6. Subcritical and supercritical pitchfork bifurcations. The bifurcations depicted in (a), (b), and (c) are subcritical, in contrast to (d), (e), and (f), which are supercritical. Solid and dashed curves denote stable and unstable branches, respectively, and each branch is labeled with its instability index. According to the definition in the text, subcritically bifurcating branches exist for values of μ at which the parent branch is less unstable (instability index 0 or $n-1$); the bifurcating branches have the same instability index (here 1 or n) as the more unstable portion of the parent branch. Note that the primary branch is unstable at the bifurcation point μ_c for the subcritical bifurcations (a), (b), and (c), and stable for the supercritical bifurcations (d) and (f); in case (e), the parent state is unstable, but to eigenvectors other than the bifurcating one. The secondary Eckhaus bifurcations discussed in this article are of type (a) and (b), whereas the primary bifurcations from the conductive state are supercritical bifurcations of type (d) and (e). There exist other, nonequivalent definitions of subcriticality, in particular requiring that the new bifurcating branches exist for values of the control parameter less than the critical value ($\mu < \mu_c$) (cases (c) and (f) only), or else where the parent branch is stable (cases (a) and (c) only). Cases (c) and (d) are the standard textbook depictions of subcritical and supercritical bifurcations, respectively, for which all three definitions coincide: the bifurcating eigenvalue of the parent branch increases with control parameter μ, and all other eigenvalues remain negative.

5. Subcriticality and center manifold reduction

In this section we will prove by center manifold reduction and normal-form analysis that the Eckhaus bifurcations are subcritical. We characterize a pitchfork bifurcation as subcritical if the bifurcating branches exist for values of the control parameter where the bifurcating eigenvalue of the parent branch is negative, as in figs. 6a, 6b, and 6c. (For the Eckhaus bifurcations, this corresponds to the statement that the mixed-mode states S_{nk} exist for μ such that $\sigma_{nk+}(\mu) < 0$, i.e. for $\mu > \mu_{nk}$.) If the bifurcation separates a stable and an unstable portion of the parent branch (cf. figs. 6a and 6c), then this definition of subcriticality coincides with various qualitative features – in particular the presence of hysteresis and of discontinuous transitions – which have been observed for the Eckhaus instability, both experimentally and in numerical simulations. We note that the literature [19, 25] contains other, nonequivalent, definitions of subcriticality (see fig. 6 and accompanying caption).

According to our definition, subcriticality can be ascertained by determining that the parent state A_n is (nonlinearly) unstable with respect to the bifurcating eigenvector a_{nk+} at the bifurcation point μ_{nk} itself. Our starting point will be the partial differential equation (4.1) derived in the previous section governing a general perturbation $a(x,t)$ to a steady solution A:

$$\frac{\partial a}{\partial t} = \mu a + \frac{\partial^2 a}{\partial x^2} - 2|A|^2 a - A^2 a^* - (2A|a|^2 + A^* a^2 + |a|^2 a). \tag{5.1}$$

By linearizing (5.1) about the pure-mode states A_n, we obtained the eigenvectors $a_{n0}(x)$ and $a_{nj\pm}(x)$ of

equations (4.14)–(4.15). From now on, we will simplify the notation by assuming a pure-mode state $A \equiv A_n$ with allowed wavenumber $Q \equiv Q_n$, and dropping the subscript n on all eigenvectors and amplitudes. Any perturbation a can be written as a linear combination of $a_0(x)$ and $a_{j\pm}(x)$ with time-dependent amplitudes $g_0(t)$ and $g_{j\pm}(t)$ as follows:

$$a(x,t) = g_0(t)\, a_0(x) + \sum_{j=1}^{\infty} g_{j-}(t)\, a_{j-}(x) + \sum_{j=1}^{\infty} g_{j+}(t)\, a_{j+}(x). \tag{5.2}$$

Eq. (5.1) governing the evolution of a leads, in principle, to a set of coupled ordinary differential equations for the amplitudes g. We seek to approximate the equation for the critical amplitude g_{k+} at the bifurcation point $\mu = \mu_{nk}$. To lowest (linear) order

$$\frac{\mathrm{d}}{\mathrm{d}t} g_{k+} = \sigma_{k+} g_{k+} = 0. \tag{5.3}$$

We now seek the next higher order correction to (5.3) which will tell us the type of bifurcation undergone by A, as well as the stability of A to a_{k+} at the bifurcation point. If the next term is quadratic in g_{k+}, the bifurcation is transcritical. If the next term is cubic, the bifurcation is a pitchfork: a negative sign corresponds to a supercritical pitchfork, a positive sign to a subcritical pitchfork. From symmetry considerations, it can already be deduced that the bifurcation is a pitchfork, but we will not need to assume this.

The full nonlinear equation governing the amplitude g_{k+} involves the amplitudes of all of the other modes, so the meaning of "the next higher order correction" in g_{k+} to (5.3) requires some clarification. On the center manifold, each of the noncritical amplitudes g_{j+} $(j \neq k)$, g_{j-}, and g_0 are functions of the critical amplitude g_{k+}. These functions can, in principle, be substituted into the equation governing g_{k+} to yield a single decoupled evolution equation involving only g_{k+} itself. In practice these functions are obtained as power series in g_{k+} whose lowest-order term is at least quadratic. The equation governing g_{k+} is locally valid on the center manifold and fully determines the bifurcation.

We follow the procedure outlined by Guckenheimer and Holmes [26]. The calculation is carried out in three stages:

(1) From the evolution equation for the critical amplitude g_{k+}, we identify the noncritical amplitudes which appear at lowest order.

(2) For each of the noncritical modes of (1), the center manifold is calculated to lowest order, i.e. approximate expressions are derived for these noncritical amplitudes in terms of the critical amplitude.

(3) The dynamics on the center manifold are calculated, i.e. the expressions of (2) are substituted into the equation derived in (1) which governs the critical amplitude.

To perform these calculations, instead of using expansion (5.2) we will find it convenient to introduce the function $f(x,t)$ and the Fourier basis $f_j(t)$ defined by

$$a(x,t) = e^{iQx} f(x,t) = e^{iQx} \sum_{j=-\infty}^{\infty} f_j(t)\, e^{ijx}. \tag{5.4}$$

From definition (4.14), clearly $f_0 = g_0$, whereas $f_{\pm j}$ and $g_{j\pm}$ are related by

$$\begin{pmatrix} f_j \\ f_{-j} \end{pmatrix} = \begin{pmatrix} \alpha_j & \beta_j \\ \beta_j & -\alpha_j \end{pmatrix} \begin{pmatrix} g_{j+} \\ g_{j-} \end{pmatrix},$$

where α_j and β_j are solutions to (4.16). In general, the expressions for $\alpha_j(\mu)$ and $\beta_j(\mu)$ are fairly complicated, but fortunately we will only require these expressions for the special case $j = k$, $\mu = \mu_{nk}$, where they take the simple forms

$$\alpha \equiv \alpha_k = -(2Q - k)/2D, \tag{5.5a}$$

$$\beta \equiv \beta_k = (2Q + k)/2D. \tag{5.5b}$$

Here

$$D \equiv \sqrt{\tfrac{1}{2}(4Q^2 + k^2)}$$

has been defined to normalize

$$\alpha^2 + \beta^2 = 1. \tag{5.6}$$

We now have the correspondence:

$$\begin{pmatrix} f_k \\ f_{-k} \end{pmatrix} = \begin{pmatrix} \alpha & \beta \\ \beta & -\alpha \end{pmatrix} \begin{pmatrix} g_{k+} \\ g_{k-} \end{pmatrix}, \tag{5.7}$$

where the matrix in (5.7) is its own inverse. Keeping in mind that one of our goals is to represent the Fourier amplitudes f_j as power series in g_{k+}, to lowest order we have

$$f_k = \alpha g_{k+}, \tag{5.8a}$$

$$f_{-k} = \beta g_{k+}. \tag{5.8b}$$

Here and in what follows, we use the equals sign interchangeably to denote equality to lowest order in g_{k+} as well as exact equality. We shall also require the following relations derived from (5.5):

$$\alpha + \beta = k/D, \tag{5.9a}$$

$$\alpha - \beta = -2Q/D. \tag{5.9b}$$

The partial differential equation obeyed by f is easily derived from (5.1) and (5.4) and can be written as:

$$\frac{\partial}{\partial t} f = -\mathscr{R}^1 - |A| \mathscr{R}^2 - \mathscr{R}^3, \tag{5.10}$$

where

$$\mathscr{R}^1 = |A|^2 (f + f^*) - \left(\frac{\partial^2}{\partial x^2} + 2iQ \frac{\partial}{\partial x} \right) f, \tag{5.11}$$

$$\mathscr{R}^2 = f^2 + 2|f|^2, \tag{5.12}$$

$$\mathscr{R}^3 = |f|^2 f \tag{5.13}$$

and by (3.12), (4.11), and (5.5)

$$|A|^2 = \mu_{nk} - Q^2 = \left(3Q^2 - \tfrac{1}{2}k^2\right) - Q^2 = \tfrac{1}{2}\left(4Q^2 - k^2\right) = -2\alpha\beta D^2 \tag{5.14}$$

Eqs. (5.4) and (5.10)–(5.13) lead to the ordinary differential equations for the individual coefficients f_j:

$$\frac{\mathrm{d}}{\mathrm{d}t} f_j = -\mathscr{R}_j^1 - |A|\mathscr{R}_j^2 - \mathscr{R}_j^3. \tag{5.15}$$

The linear term obtained by substituting (5.4) into (5.11) is:

$$\mathscr{R}_j^1 = \left[|A|^2 + j(j + 2Q)\right]f_j + |A|^2 f_{-j}. \tag{5.16}$$

To compute the form of $\mathscr{R}_j^2$, we use (5.4) to write

$$f^2 = \sum_{l=-\infty}^{\infty} f_l \, \mathrm{e}^{ilx} \sum_{m=-\infty}^{\infty} f_m \, \mathrm{e}^{imx} = \sum_{j=-\infty}^{\infty} \mathrm{e}^{ijx} \sum_{m=-\infty}^{\infty} f_m f_{j-m},$$

$$|f|^2 = \sum_{l=-\infty}^{\infty} f_l \, \mathrm{e}^{-ilx} \sum_{m=-\infty}^{\infty} f_m \, \mathrm{e}^{imx} = \sum_{j=-\infty}^{\infty} \mathrm{e}^{ijx} \sum_{m=-\infty}^{\infty} f_m f_{j+m},$$

which, when substituted into (5.12) yields

$$\mathscr{R}_j^2 = \sum_{m=-\infty}^{\infty} f_m\left(f_{j-m} + 2f_{j+m}\right). \tag{5.17}$$

Similarly, expanding (5.13),

$$\mathscr{R}^3 = |f|^2 f = \sum_{j=-\infty}^{\infty} \mathrm{e}^{ijx} \sum_{l=-\infty}^{\infty} \sum_{m=-\infty}^{\infty} f_l f_m f_{l+m-j},$$

leads to

$$\mathscr{R}_j^3 = \sum_{l=-\infty}^{\infty} \sum_{m=-\infty}^{\infty} f_l f_m f_{l+m-j}. \tag{5.18}$$

We are now in a position to carry out the first stage of the center manifold calculation, that of determining which of the noncritical amplitudes appear to leading order in the evolution equation for the critical amplitude. To translate to the Fourier basis, we recall that $f_0 = g_0$ and that for fixed j, $f_{\pm j}$ and $g_{j\pm}$ are related by the matrix multiplication of (5.7). We can therefore consider instead the evolution equations for f_{+k} and f_{-k}, a linear combination of which forms the evolution equation for g_{k+}. Clearly, by (5.8), f_{+k} and f_{-k} depend linearly on g_{k+} to leading order. To determine the functional dependence of the other Fourier amplitudes, we recall that $g_{j\pm}$ $(j \neq k)$ and g_0 have a quadratic or higher-order dependence on g_{k+}. The power series for the Fourier amplitudes $f_{\pm j}$ $(j \neq k)$, which are linear combinations of $g_{j\pm}$, and for $f_0 = g_0$, must therefore also begin with a quadratic or higher-order term.

We therefore write

$$\frac{d}{dt}\begin{pmatrix} f_k \\ f_{-k} \end{pmatrix} = -\begin{pmatrix} \mathscr{R}_k^1 \\ \mathscr{R}_{-k}^1 \end{pmatrix} - |A|\begin{pmatrix} \mathscr{R}_k^2 \\ \mathscr{R}_{-k}^2 \end{pmatrix} - \begin{pmatrix} \mathscr{R}_k^3 \\ \mathscr{R}_{-k}^3 \end{pmatrix} \tag{5.19}$$

and seek the terms in the right-hand side of (5.19) which will contribute to lowest order in g_{k+}, i.e. the terms in $\mathscr{R}_{\pm k}^2$ and $\mathscr{R}_{\pm k}^3$ which involve $f_{\pm k}$ in preference to the other Fourier amplitudes.

Let us begin by considering the cubic term $\mathscr{R}_{\pm k}^3$ as defined by (5.18). The terms $f_l f_m f_{l+m-k}$ and $f_l f_m f_{l+m+k}$ will be of cubic order if all of l, m, and $l + m \pm k = \pm k$. We find

$$\mathscr{R}_k^3 = \sum_{l=-\infty}^{\infty} \sum_{m=-\infty}^{\infty} f_l f_m f_{l+m-k} = f_k^3 + 2f_k f_{-k}^2, \tag{5.20a}$$

$$\mathscr{R}_{-k}^3 \sum_{l=-\infty}^{\infty} \sum_{m=-\infty}^{\infty} f_l f_m f_{l+m+k} = f_{-k}^3 + 2f_{-k} f_k^2. \tag{5.20b}$$

(Recall that we use the equals sign to denote equality to lowest order in g_{k+} as well as strict equality.)

Now consider expression (5.17) for the quadratic term $\mathscr{R}_{\pm k}^2$. In the terms $f_m(2f_{\pm k+m} + f_{\pm k-m})$ and $f_m(2f_{-k+m} + f_{-k-m})$, both m and $\pm k \pm m$ cannot simultaneously take on the values $\pm k$. Thus the lowest-order terms will be those in which either $m = \pm k$, or $\pm k \pm m = \pm k$. The products will again be of cubic or higher order,

$$\mathscr{R}_k^2 = \sum_{m=-\infty}^{\infty} f_m(2f_{k+m} + f_{k-m})$$
$$= f_k(2f_{2k} + f_0) + f_{-k}(2f_0 + f_{2k}) + f_0(2f_k + f_k) + f_{2k}f_{-k} + 2f_{-2k}f_{-k}$$
$$= 2f_0(2f_k + f_{-k}) + 2(f_k f_{2k} + f_{-k}f_{-2k} + f_{-k}f_{2k}), \tag{5.21a}$$

$$\mathscr{R}_{-k}^2 = \sum_{m=-\infty}^{\infty} f_m(2f_{-k+m} + f_{-k-m})$$
$$= f_k(2f_0 + f_{-2k}) + f_{-k}(2f_{-2k} + f_0) + f_0(2f_{-k} + f_{-k}) + 2f_{2k}f_k + f_{-2k}f_k$$
$$= 2f_0(2f_{-k} + f_k) + 2(f_{-k}f_{-2k} + f_k f_{2k} + f_k f_{-2k}). \tag{5.21b}$$

The linear terms $\mathscr{R}_{\pm k}^1$ of (5.16) and the cubic terms $\mathscr{R}_{\pm k}^2$ of (5.20) involve only $f_{\pm k}$. We see from (5.20) and (5.21) that the only other amplitudes of interest are $f_{\pm 2k}$ and f_0. This completes the first stage of the center manifold calculation.

In the second stage of the center manifold calculation, we calculate the dependence of the relevant amplitudes $f_{\pm 2k}$ and f_0 on g_{k+}. This is done by solving (5.15), for $j = \pm 2k, 0$ to lowest order in g_{k+}. The time dependence vanishes at lowest order, and we seek steady-state solutions of (5.15), that is, we solve

$$0 = -\mathscr{R}_j^1 - |A|\mathscr{R}_j^2 - \mathscr{R}_j^3$$

or

$$\mathscr{R}_j^1 = -|A|\mathscr{R}_j^2 - \mathscr{R}_j^3 \tag{5.22}$$

to lowest order in g_{k+}.

We now carry out this procedure for f_0. As before, the lowest-order terms are those that contain the maximum number of powers of $f_{\pm k}$. For $\mathscr{R}_0^2$ these terms are

$$
\mathscr{R}_0^2 = \sum_{m=-\infty}^{\infty} f_m(f_{-m} + 2f_m) = f_k(f_{-k} + 2f_k) + f_{-k}(f_k + 2f_{-k})
$$

$$
= 2(f_k^2 + f_k f_{-k} + f_{-k}^2) = 2(\alpha^2 + \alpha\beta + \beta^2)g_{k+}^2 \tag{5.23}
$$

where we have used (5.17) and (5.8).

The lowest-order terms in $\mathscr{R}_0^3$ are necessarily cubic in g_{k+}, and so can be ignored. From the linear analysis, we have eqs. (5.16) and more specifically (4.13), leading to

$$
\mathscr{R}_0^1 = 2|A|^2 f_0. \tag{5.24}
$$

Substituting (5.23) and (5.24) into (5.22), we obtain

$$
2|A|^2 f_0 = -|A|2(\alpha^2 + \alpha\beta + \beta^2)g_{k+}^2,
$$

leading to

$$
f_0 = -\frac{1}{|A|}(\alpha^2 + \alpha\beta + \beta^2)g_{k+}^2. \tag{5.25}
$$

The calculation for $f_{\pm 2k}$ is complicated by coupling between f_{2k} and f_{-2k}. The lowest-order terms are again quadratic in g_{k+} and, with the help of relations (5.8) are written as

$$
\mathscr{R}_{2k}^2 = \sum_{m=-\infty}^{\infty} f_m(f_{2k-m} + 2f_{2k+m}) = f_k(f_k + 2f_{-k}) = \alpha(\alpha + 2\beta)g_{k+}^2, \tag{5.26a}
$$

$$
\mathscr{R}_{-2k}^2 = \sum_{m=-\infty}^{\infty} f_m(f_{-2k-m} + 2f_{-2k+m}) = f_{-k}(f_{-k} + 2f_k) = \beta(\beta + 2\alpha)g_{k+}^2. \tag{5.26b}
$$

$\mathscr{R}_{\pm 2k}^3$ is again not considered because it is of higher order in g_{k+}. The linear term coupling f_{2k} and f_{-2k} can be written using (5.16), (5.14), and (5.9) as

$$
\begin{pmatrix} \mathscr{R}_{+2k}^1 \\ \mathscr{R}_{-2k}^1 \end{pmatrix} = \begin{pmatrix} |A|^2 + 4k(k+Q) & |A|^2 \\ |A|^2 & |A|^2 + 4k(k-Q) \end{pmatrix} \begin{pmatrix} f_{+2k} \\ f_{-2k} \end{pmatrix}
$$

$$
= 2D^2 \begin{pmatrix} \alpha^2 + 3\alpha\beta + 3\beta^2 & -\alpha\beta \\ -\alpha\beta & 3\alpha^2 + 3\alpha\beta + \beta^2 \end{pmatrix} \begin{pmatrix} f_{+2k} \\ f_{-2k} \end{pmatrix}. \tag{5.27}
$$

Using (5.26) and (5.27), eq. (5.22) becomes

$$
2D^2 \begin{pmatrix} \alpha^2 + 3\alpha\beta + 3\beta^2 & -\alpha\beta \\ -\alpha\beta & 3\alpha^2 + 3\alpha\beta + \beta^2 \end{pmatrix} \begin{pmatrix} f_{+2k} \\ f_{-2k} \end{pmatrix} = -|A| \begin{pmatrix} \alpha(\alpha + 2\beta) \\ \beta(\beta + 2\alpha) \end{pmatrix} g_{k+}^2. \tag{5.28}
$$

Inverting the matrix on the left-hand side of (5.28) and using (5.14), we obtain

$$
\begin{pmatrix} f_{+2k} \\ f_{-2k} \end{pmatrix} = \frac{-|A|}{2D^2(\alpha + \beta)} \begin{pmatrix} \alpha \\ \beta \end{pmatrix} g_{k+}^2 = \frac{\alpha\beta}{|A|(\alpha + \beta)} \begin{pmatrix} \alpha \\ \beta \end{pmatrix} g_{k+}^2 .
\tag{5.29}
$$

This terminates the second stage of the center manifold reduction.

We are now ready to carry out the third state of the calculation by substituting expressions (5.8), (5.25), and (5.29) for $f_{\pm k}$, f_0 and $f_{\pm 2k}$ into (5.19). Multiplying (5.19) by the matrix of (5.7) (recall that this matrix is its own inverse), we obtain:

$$
\frac{\mathrm{d}}{\mathrm{d}t} \begin{pmatrix} g_{k+} \\ g_{k-} \end{pmatrix} = \begin{pmatrix} \alpha & \beta \\ \beta & -\alpha \end{pmatrix} \frac{\mathrm{d}}{\mathrm{d}t} \begin{pmatrix} f_k \\ f_{-k} \end{pmatrix}
$$

$$
= \begin{pmatrix} \alpha & \beta \\ \beta & -\alpha \end{pmatrix} \left[- \begin{pmatrix} \mathscr{R}_k^1 \\ \mathscr{R}_{-k}^1 \end{pmatrix} - |A| \begin{pmatrix} \mathscr{R}_k^2 \\ \mathscr{R}_{-k}^2 \end{pmatrix} - \begin{pmatrix} \mathscr{R}_k^3 \\ \mathscr{R}_{-k}^3 \end{pmatrix} \right].
$$

We require only the first of these equations:

$$
\frac{\mathrm{d}}{\mathrm{d}t} g_{k+} = -|A|\left(\alpha\mathscr{R}_k^2 + \beta\mathscr{R}_{-k}^2\right) - \left(\alpha\mathscr{R}_k^3 + \beta\mathscr{R}_{-k}^3\right),
\tag{5.30}
$$

where we have set the linear term to zero, since g_{k+} is the critical mode.

We begin by using (5.21), (5.8), (5.25), and (5.29) to write the quadratic terms $\mathscr{R}_{\pm k}^2$ as

$$
\mathscr{R}_k^2 = 2f_0(2f_k + f_{-k}) + 2(f_k f_{2k} + f_{2k} f_{-k} + f_{-k} f_{-2k})
$$

$$
= -\frac{2}{|A|}(\alpha^2 + \alpha\beta + \beta^2)(2\alpha + \beta)g_{k+}^3 + \frac{2\alpha\beta}{|A|(\alpha + \beta)}(\alpha^2 + \alpha\beta + \beta^2)g_{k+}^3,
$$

$$
\mathscr{R}_{-k}^2 = 2f_0(2f_{-k} + f_k)g_{k+} + 2(f_k f_{2k} + f_k f_{-2k} + f_{-k} f_{-2k})
$$

$$
= -\frac{2}{|A|}(\alpha^2 + \alpha\beta + \beta^2)(2\beta + \alpha)g_{k+}^3 + \frac{2\alpha\beta}{|A|(\alpha + \beta)}(\alpha^2 + \alpha\beta + \beta^2)g_{k+}^3 .
$$

The linear combination we require in (5.30) becomes

$$
\alpha\mathscr{R}_k^2 + \beta\mathscr{R}_{-k}^2
$$

$$
= -\frac{1}{|A|}\{2[\alpha(2\alpha + \beta) + \beta(2\beta + \alpha)] - 2\alpha\beta\}(\alpha^2 + \alpha\beta + \beta^2)g_{k+}^3
$$

$$
= -\frac{1}{|A|}(4\alpha^2 + 2\alpha\beta + 4\beta^2)(\alpha^2 + \alpha\beta + \beta^2)g_{k+}^3 .
$$

We use (5.6) to simplify

$$
\alpha\mathscr{R}_k^2 + \beta\mathscr{R}_{-k}^2 = -\frac{1}{|A|}(4 + 2\alpha\beta)(1 + \alpha\beta)g_{k+}^3
$$

$$
= -\frac{1}{|A|}(4 + 6\alpha\beta + 2\alpha^2\beta^2)g_{k+}^3 .
\tag{5.31}
$$

Turning now to the cubic terms $\mathscr{R}^3_{\pm k}$, we find using (5.20), (5.8), and (5.6) that

$$\mathscr{R}^3_k = f^3_k + 2f_k f^2_{-k} = \alpha(\alpha^2 + 2\beta^2)g^3_{k+} = \alpha(1 + \beta^2)g^3_{k+} \,,$$

$$\mathscr{R}^3_{-k} = f^3_{-k} + 2f_{-k}f^2_k = \beta(\beta^2 + 2\alpha^2)g^3_{k+} = \beta(1 + \alpha^2)g^3_{k+} \,.$$

Again making use of (5.6) we obtain for their linear combination

$$\alpha\mathscr{R}^3_k + \beta\mathscr{R}^3_{-k} = \left[\alpha^2(1 + \beta^2) + \beta^2(1 + \alpha^2)\right]g^3_{k+}$$

$$= (1 + 2\alpha^2\beta^2)g^3_{k+} \,. \tag{5.32}$$

We now add the quadratic terms (5.31) and the cubic terms (5.32) into (5.30):

$$\frac{\mathrm{d}}{\mathrm{d}t}g_{k+} = -|A|\left(\alpha\mathscr{R}^2_k + \beta\mathscr{R}^2_{-k}\right) - \left(\alpha\mathscr{R}^3_k + \beta\mathscr{R}^3_{-k}\right)$$

$$= \left[(4 + 6\alpha\beta + 2\alpha^2\beta^2) - (1 + 2\alpha^2\beta^2)\right]g^3_{k+}$$

$$= 3(1 + 2\alpha\beta)g^3_{k+} \,.$$

We use (5.6) and (5.9a) to write the expression in parentheses above as:

$$1 + 2\alpha\beta = \alpha^2 + \beta^2 + 2\alpha\beta = (\alpha + \beta)^2 = k^2/D^2 \,.$$

Hence we obtain as the sought-after lowest-order evolution equation for g_{k+}:

$$\frac{\mathrm{d}}{\mathrm{d}t}g_{k+} = \sigma_{k+}g_{k+} + \frac{3k^2}{D^2}g^3_{k+} \,. \tag{5.33}$$

The magnitude of the cubic coefficient in (5.33) depends on the normalization chosen for the critical eigenvector a_{k+}, and is therefore not significant. Its positive sign, however, is invariant, and proves that the bifurcation is subcritical.

6. Relation between the primary and secondary eigenvectors

Just prior to the point of bifurcation μ_n, the conductive branch C has n unstable eigenmodes c_m ($0 \le m \le n - 1$) resulting from the previous pitchfork bifurcations at μ_m. Just after the bifurcation point, the branch A_n exists, also with n unstable eigenmodes, a property which it inherits from the conductive branch. These unstable eigenmodes a_{nk+} ($1 \le k \le n$) restabilize one by one at the critical values μ_{nk}. We will now clarify the connection between the destabilizing eigenmodes c_n of C, and the restabilizing eigenmodes a_{nk+} of A_n.

Consider following a path of steady states which coincides with C for $\mu < \mu_n$ and then switches onto the branch A_n for $\mu > \mu_n$, as in fig. 7a. Along this path, both the eigenvectors and eigenvalues should vary continuously with μ (but not smoothly: the first derivatives will be discontinuous at the bifurcation point μ_n). We should therefore be able to find a correspondence between the eigenvectors c_m and eigenvalues λ_m of $A = 0$, and the eigenvectors $a_{nk\pm}$ and eigenvalues $\sigma_{nk\pm}$ of A_n.
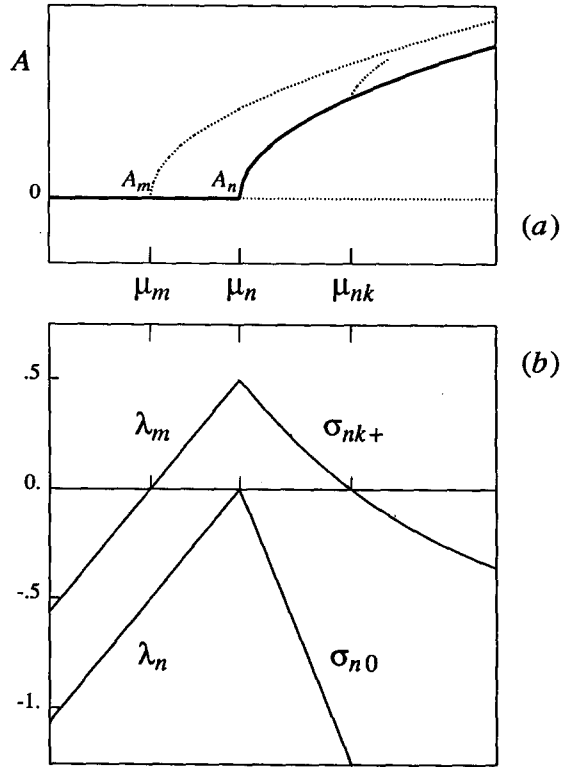
Fig. 7. Connection between the primary and secondary instabilities. (a) Bifurcation diagram. The bold curve indicates the path of steady states discussed in section 6. For $\mu \leq \mu_n$, the path follows the conductive state C; for $\mu \geq \mu_n$, we follow the branch A_n. The dotted curves are additional branches A_m and S_{nk}, originating at bifurcation points μ_m and μ_{nk}. (b) Eigenvalues as a function of μ. Below μ_n, the eigenvalues λ_m and λ_n of C are plotted. Above μ_n, the eigenvalues σ_{nk+} (where $k = |Q_n - Q_m|$) and σ_{n0} of A_n is plotted. λ_m and σ_{nk+} cross zero at the destabilizing bifurcation point μ_m and the restabilizing bifurcation point μ_{nk}, respectively. The eigenvalues (and corresponding eigenvectors) join continuously (but not smoothly) at μ_n, indicating that the destabilizing direction of C at μ_m is connected to the stabilizing direction of A_n at μ_{nk}. The eigenvalue λ_n which is marginal at μ_n is connected to σ_{n0}. The correspondence between the other eigenvalues of A and C at μ_n is given by (6.2). The numerical values used in this figure have been calculated from the case $m = 0$, $n = 1$, and $k = 1$, illustrated in the phase portraits of figs. $3\alpha-3\delta$.

For the $k = 0$ eigenmodes, referring to (3.9), (3.11), (4.12), and (4.14) or to table 1 of the appendix we have

$$a_{n0} = e^{iQ_n x} = c_n$$

and at $\mu = \mu_n$

$$\sigma_{n0} = 0 = \lambda_n.$$

The eigenvalue of C which changes sign at $\mu = \mu_n$, causing the bifurcation and creating state A_n, is λ_n. Its corresponding eigenvector $c_n = e^{iQ_n x}$ is equal to a_{n0}, not only at the bifurcation point, but for all $\mu \geq \mu_n$. The eigenvalues are no longer equal for $\mu \geq \mu_n$; however, λ_n continues to increase from zero, while σ_{n0} becomes negative (see fig. 7b).

Analyzing the $k > 0$ modes is less trivial. However, at μ_n, the point at which A_n branches from 0, the expressions for the eigenvalues and eigenvectors reduce to a particularly simple form:

$$\sigma_{nk\pm} = -k^2 \pm 2k|Q_n|.$$

Eq. (4.16) becomes

$$\begin{pmatrix} \pm 2k|Q_n| + 2kQ_n & 0 \\ 0 & \pm 2k|Q_n| - 2kQ_n \end{pmatrix} \begin{pmatrix} \alpha \\ \beta \end{pmatrix} = \begin{pmatrix} 0 \\ 0 \end{pmatrix}. \tag{6.1}$$

We assume $|Q_n| > 0$. Eq. (6.1) implies that only one of α and β is nonzero, according to the sign of Q_n and to the choice of eigenvalue $\sigma_{\pm}$. If $Q_n > 0$, and $\sigma = \sigma_+$, or if $Q_n < 0$, and $\sigma = \sigma_-$, then the coefficient multiplying $e^{i(Q_n + k)x}$ is 0, so that $a_{nk\pm} = e^{i(Q_n - k)x}$. In this case, equality of eigenvectors c_m and $a_{nk\pm}$ is achieved if $Q_m = Q_n - k$, or $k = Q_n - Q_m$. Since $k > 0$, $Q_n > Q_m$ is required. Similarly, if $Q_n > 0$, and $\sigma = \sigma_-$, or if $Q_n < 0$, and $\sigma = \sigma_+$, then the coefficient multiplying $e^{i(Q_n - k)x}$ is 0, so that $a_{nk\pm} = e^{i(Q_n + k)x} = c_m$ if $Q_m = Q_n + k$, or $k = Q_m - Q_n$, with $Q_m > Q_n$.

This information can all be summarized more succinctly as follows. At $\mu = \mu_n$, with $k = |Q_n - Q_m|$:

$$c_m = a_{nk+} \quad \text{if } |Q_m| < |Q_n| \text{ or } Q_m Q_n \le 0, \text{ i.e. if } m < n \text{ or } m + n \text{ odd,} \tag{6.2a}$$

$$c_m = a_{nk-} \quad \text{if } |Q_m| > |Q_n| \text{ and } Q_m Q_n > 0, \text{ i.e. if } m > n \text{ and } m + n \text{ even,} \tag{6.2b}$$

$$c_n = a_{n0} \quad \text{if } Q_n = Q_m, \text{ i.e. if } m = n. \tag{6.2c}$$

In particular, if we recall that the n destabilizing eigenvectors of C prior to the bifurcation point μ_n are c_m, with $|Q_m| < |Q_n|$, we see by (6.2a) that these are connected to the restabilizing eigenvectors of the branch A_n (i.e. a_{nk+} with $k \le 2|Q_n|$), provided that $k = |Q_n - Q_m|$.

Fig. 7b illustrates the connection between eigenvalues λ_m and σ_{nk+} for the specific values $m = 0$, $n = 1$, and $k = 1$, corresponding to the restabilization of branch A_1. This is the same case that is shown schematically in fig. 3δ, where the eigenvectors c_0 and a_{11+}, which coincide at $\mu = \mu_1$ (i.e. at a value of μ between those of figs. 3β and 3γ), are represented as parallel. Tables 2–6 of the appendix also list correspondences calculated from (6.2).

Table 6

Correspondence between eigenvectors of C and of A_n. Entry of $k \pm$ or 0 at (n, m) means that $c_m = a_{nk\pm}$ or $c_m = a_{n0}$ at $\mu = \mu_n$. Along the diagonal are the eigenvectors which bifurcate at μ_n. Below the diagonal are the eigenvectors which play a role in the Eckhaus instability, i.e. the destabilizing eigenvectors of C and the restabilizing eigenvectors of A_n. Above the diagonal are eigenvectors whose eigenvalues remain negative along paths which switch from C to A_n. See (6.2) and fig. 7.

n	m						
0	0	1	2	3	4	5	6
0	0	1 +	1 −	2 +	2 −	3 +	3 −
1	1 +	0	2 +	1 −	3 +	2 −	4 +
2	1 +	2 +	0	3 +	1 −	4 +	2 −
3	2 +	1 +	3 +	0	4 +	1 −	5 +
4	2 +	3 +	1 +	4 +	0	5 +	1 −
5	3 +	2 +	4 +	1 +	5 +	0	6 +
6	3 +	4 +	2 +	5 +	1 +	6 +	0

7. Periodic boundary conditions

In a periodic domain, the location of the boundaries is not significant: a solution translated in x by an arbitrary distance, or phase, remains a solution. Thus, for every allowed wavenumber Q, there now exists a continuum – a circle parametrized by ϕ – of pure-mode states:

$$A = \sqrt{\mu - Q^2}\, e^{i(Q_n x + \phi)}, \tag{7.1}$$

where ϕ can now take on any value between 0 and 2π. The ϕ-circles of solutions for different values of Q are located on planes which are mutually perpendicular, making pictorial representation of more than one such circle impossible. The corresponding velocity w defined in (3.4) has arbitrary phase, or equivalently, is a linear combination which includes sine as well as cosine:

$$
\begin{aligned}
w(x) &= 2|A|\cos[(Q_c + Q)x + \phi] \\
&= 2|A|\{\cos\phi\cos[(Q_c + Q)x] - \sin\phi\cos[(Q_c + Q)x]\}.
\end{aligned}
$$

The multiplicity of each of the eigenvalues λ_n, σ_{n0}, σ_{nk+}, and σ_{nk-} is doubled. Corresponding to λ_n, one now has two eigenvectors $e^{iQ_n x}$ and $i e^{iQ_n x}$. (These are linearly independent over the reals, as are $\sin(Q_n x)$ and $\cos(Q_n x)$: one should consider $A = (\text{Re}(A), \text{Im}(A))$ as belonging to a two-dimensional real vector space whose components are coupled via (3.1).) For the pure-mode state (7.1) of phase ϕ, the eigenvectors associated to the eigenvalue σ_{n0} are $e^{i(Q_n x + \phi)}$ and $i e^{i(Q_n x + \phi)}$. The eigenvectors $a_{nk\pm}$ defined by (4.15) must also be multiplied by $e^{i\phi}$.

Before stating the additional eigenvectors associated with $\sigma_{nk\pm}$, we first demonstrate the source of the requirement that α and β in (4.3)–(4.4) be real in the free-slip case. The condition on the real parts of α and β is derived from applying (3.2) to expression (4.3) at $x = \pi$. This leads to the expression

$$\sin(k\pi)\left[(Q_c + Q + k)\,\text{Re}(\alpha) - (Q_c + Q - k)\,\text{Re}(\beta)\right] = 0,$$

which can be satisfied by taking k integer. On the other hand, the condition on the imaginary parts of α and β results from applying the free-slip condition (3.2) at $x = 0$, yielding

$$(Q_c + Q + k)\,\text{Im}(\alpha) + (Q_c + Q - k)\,\text{Im}(\beta) = 0,$$

a constraint which, barring exceptional values of Q_c, Q, k, and μ, is incompatible with the equation (see (7.2) below) satisfied by eigenvectors. Thus, in the free-slip case, $\text{Im}(\alpha) = \text{Im}(\beta) = 0$.

In the case of periodic boundary conditions (3.3), k need only be integer and α and β may be complex. Their real and imaginary parts satisfy decoupled systems. The system for $(\text{Re}(\alpha), \text{Re}(\beta))$ is (4.4), while that for $(\text{Im}(\alpha), \text{Im}(\beta))$ differs from (4.4) in its off-diagonal elements:

$$
\begin{pmatrix} \sigma & 0 \\ 0 & \sigma \end{pmatrix}
\begin{pmatrix} \text{Im}(\alpha) \\ \text{Im}(\beta) \end{pmatrix}
= -\begin{pmatrix} \mu - Q^2 + k^2 + 2kQ & -(\mu - Q^2) \\ -(\mu - Q^2) & \mu - Q^2 + k^2 - 2kQ \end{pmatrix}
\begin{pmatrix} \text{Im}(\alpha) \\ \text{Im}(\beta) \end{pmatrix}. \tag{7.2}
$$

The eigenvalues $\sigma_{nk\pm}$ of (7.2) are identical to those of the system (4.4), but one derives the additional

eigenvectors

$$b_{nk+}(\mu) \equiv i e^{i(Q_n x + \phi)} \left[-\alpha_{nk}(\mu) e^{ikx} + \beta_{nk}(\mu) e^{-ikx} \right],$$ (7.3a)

$$b_{nk-}(\mu) \equiv i e^{i(Q_n x + \phi)} \left[\beta_{nk}(\mu) e^{ikx} + \alpha_{nk}(\mu) e^{-ikx} \right],$$ (7.3b)

where $\alpha_{nk}(\mu)$ and $\beta_{nk}(\mu)$ retain their definitions (4.16).

The primary and secondary bifurcations remain supercritical and subcritical pitchforks, respectively, but of a slightly different nature: they are "pitchforks of revolution" rather than two discrete branches. The analysis of section 5 must be altered to include the additional modes: expansion (5.2) is enlarged to read

$$a(x,t) = g_0(t) a_0(x) + \sum_{j=1}^{\infty} g_{j-}(t) a_{j-}(x) + \sum_{j=1}^{\infty} g_{j+}(t) a_{j+}(x)$$

$$+ h_0(t) b_0(x) + \sum_{j=1}^{\infty} h_{j-}(t) b_{j-}(x) + \sum_{j=1}^{\infty} h_{j+}(t) b_{j+}(x).$$

The Fourier expansion (5.4) is retained, but the Fourier amplitudes f_j are now complex. Because there are now two critical modes $a_{k+}(x)$ and $b_{k+}(x)$, with corresponding critical amplitudes $g_{k+}(t)$ and $h_{k+}(t)$, the center manifold is two-dimensional: all noncritical amplitudes are represented as functions of both g_{k+} and h_{k+}. Calculations analogous to those for the free-slip case lead to the replacement of (5.33) by the pair of coupled equations

$$\frac{d}{dt} \begin{pmatrix} g_{k+} \\ h_{k+} \end{pmatrix} = \sigma_{k+} \begin{pmatrix} g_{k+} \\ h_{k+} \end{pmatrix} + \frac{3k^2}{D^2} (g_{k+}^2 + h_{k+}^2) \begin{pmatrix} g_{k+} \\ h_{k+} \end{pmatrix},$$ (7.4)

which is the normal form for a subcritical pitchfork bifurcation with rotational symmetry.

8. Discussion

In this article, we have shown that the Eckhaus instability in a finite domain is the last of a series of secondary bifurcations undergone by the pure-mode states. When the state A_n, with wavenumber Q_n, bifurcates from the conductive state C, C has n unstable directions. A_n inherits these unstable directions and, in order to become stable, must undergo n secondary pitchfork bifurcations, accompanied by the formation of mixed-mode states. The essential features of these secondary bifurcations are:

(1) Each secondary bifurcation restabilizes its parent branch A_n to one unstable direction, decreasing its instability index by one.

(2) The secondary bifurcations result from mode interactions between primary pure-mode states, as described in refs. [19, 22, 23].

(3) The secondary bifurcations are all subcritical. As a consequence, the mixed-mode branches S_{nk} exist only for $\mu > \mu_{nk}$ and are necessarily all unstable in the absence of any subsequent bifurcations.

(4) Each restabilizing bifurcation of A_n corresponds to one of the destabilizing supercritical bifurcations of C responsible for the formation of other pure-mode states.

One of the consequences of our analysis is a confirmation of the length-independent downwards shift (4.17) of the Eckhaus parabola for a finite geometry, derived by Kramer and Zimmerman [7] and observed experimentally by Ahlers et al. [15]. We mention here that some of the bifurcation-theoretic results we have obtained are briefly alluded to in ref. [11], and also, that while preparing this manuscript, we became aware of a parallel investigation by Tsiveriotis and Brown [27] using the Swift–Hohenberg equation. However, Tsiveriotis and Brown treat only integer Q_c, and also do not derive the deviation (4.17) from the classic infinite-length Eckhaus formula.

In analyzing the stability of both the pure-mode and the mixed-mode states, we have been guided by a basic property of pitchfork bifurcations, namely, that a bifurcating branch inherits the spectrum and, in particular, the unstable directions, of its parent state (see fig. 6). This principle depends on two necessary conditions: (i) the discreteness of the spectrum and (ii) its continuous dependence on μ over a continuous path of steady states, even when following a path that switches branches at the bifurcation point (see fig. 7a). This ensures that eigenvalues of the parent branch which are negative or positive at the bifurcation point will remain so for the bifurcating branch over some finite interval of the parameter μ. More extensive use of the inheritance of spectra could potentially prove useful in problems which are less analytically tractable, such as the nonperiodic domains studied in refs. [8, 9]. Such an analysis is, of course, valid only locally near a bifurcation point: a finite distance away, an eigenvalue of a branch may change sign, causing it to undergo a bifurcation and change its instability index.

In future work, we will describe the mixed-mode states selected by our boundary conditions. More fundamentally, we plan to address the role played by symmetry. When a system is perturbed in such a way as to break its symmetry, pitchfork bifurcations become "imperfect", and are transformed to saddle–node bifurcations: here too, the eigenvalues should evolve continuously as the imperfection is introduced. This is only the most obvious consequence: branches can move, disappear, merge, and intersect in unexpected ways, some of which can lead to time-dependent behavior. Here too, the steady states and spectra should evolve continuously as the symmetry of the domain is progressively decreased. We believe that we have already observed remnants of the Eckhaus instability in our previous numerical studies of axisymmetric spherical Couette flow [28] and cylindrical convection [29]. We hope to verify our interpretation and to be able to characterize a generalized Eckhaus instability.

Acknowledgements

References

[1] W. Eckhaus, Studies in Nonlinear Stability Theory (Springer, Berlin, 1965).
[2] A.C. Newell and J. Whitehead, J. Fluid Mech. 38 (1969) 279.
[3] L.A. Segel, J. Fluid Mech. 38 (1969) 203.

[4] A. Zippelius and E. Siggia, Phys. Fluids 26 (1983) 2905.

[5] M.C. Cross and A.C. Newell, Physica D 10 (1984) 299.

[6] Y. Pomeau and P. Manneville, J. Phys. Lett. 40 (1979) 609.

[7] L. Kramer and W. Zimmerman, Physica D 16 (1985) 221.

[8] P.G. Daniels, Mathematika 25 (1978) 216; Proc. R. Soc. London Ser. A 358 (1977) 173; Proc. R. Soc. London Ser. A 378 (1981) 539.

[9] M.C. Cross, P.G. Daniels, P.C. Hohenberg and E.D. Siggia, J. Fluid Mech. 127 (1983) 15.

[10] S. Zaleski, J. Fluid Mech. 149 (1984) 101.

[11] Y. Pomeau and S. Zaleski, J. Phys. Paris 42 (1981) 515.

[12] H. Riecke and H.-G. Paap, Phys. Rev. A 33 (1986) 547.

[13] P. Coullet and L. Gil, preprint;
P. Coullet and S. Fauve, Phys. Rev. Lett. 55 (1985) 2857.

[14] V. Croquette, Thesis, Université Pierre et Marie Curie (1986);
A. Pocheau, Thesis, Université Pierre et Marie Curie (1983).

[15] G. Ahlers, D.S. Cannell, M.A. Dominguez-Lerma and R. Heinrichs, Physica D 23 (1986) 202.

[16] M. Lowe and J.P. Gollub, Phys. Rev. Lett. 55 (1985) 2575.

[17] B. Matkowsky, private communication.

[18] J. Leray and Schauder, Ann. Sci. Ecole Norm. Sup. Ser. 3, 51 (1934) 45;
T.B. Benjamin, Math. Proc. Camb. Phil. Soc. 79 (1976) 373.

[19] M. Golubitsky and D. Schaeffer, Singularities and Groups in Bifurcation Theory, Vol. I (Springer, Berlin, 1985);
M. Golubitsky, D. Schaeffer, and I. Stewart, Singularities and Groups in Bifurcation Theory, Vol. II (Springer, Berlin, 1988).

[20] V.I. Arnol'd, Geometrical Methods in the Theory of Ordinary Differential Equations (Springer, Berlin, 1983).

[21] J. Palis and W. de Melo, Geometric Theory of Dynamical Systems (Springer, Berlin, 1982).

[22] L. Bauer, H.B. Keller and E.L. Reiss, SIAM Rev. (1975) 17, 101.

[23] J.P. Keener, Stud. Appl. Math. (1976) 55, 187;
D. Schaeffer, Math. Proc. Camb. Phil. Soc. (1980) 87, 307;
M. Shearer, SIAM J. Math. Anal. (1980) 11, 365;
D.S. Riley and K.H. Winters, J. Fluid Mech. (1989) 204, 325.

[24] R. Seydel, ZAMP (1975) 26, 713.

[25] R. Seydel, From Equilibrium to Chaos: Practical Bifurcation and Stability Analysis (Elsevier, New York, 1988).

[26] J. Guckenheimer and P. Holmes, Nonlinear Oscillations, Dynamical Systems, and Bifurcations of Vector Fields (Springer, New York, 1983).

[27] K. Tsiveriotis and R.A. Brown, Phys. Rev. Lett. 63 (1989) 2048;
L.S. Tuckerman and D. Barkley, Phys. Rev. Lett., submitted for publication.

[28] P.S. Marcus and L.S. Tuckerman, J. Fluid Mech. 185 (1987) 31.

[29] L.S. Tuckerman and D. Barkley, Phys. Rev. Lett. 61 (1988) 408;
D. Barkley and L.S. Tuckerman, Physica D 37 (1989) 288.